Review of Scientific Instruments

Development of an experimental facility for the study of microparticle initiated radio frequency vacuum breakdown

Cite as: Rev. Sci. Instrum. **92**, 013508 (2021); https://doi.org/10.1063/5.0034559
Submitted: 21 October 2020 . Accepted: 23 December 2020 . Published Online: 21 January 2021

R. Casagrande, H. Faugel, F. Fischer, H. Fünfgelder, F. Riedl, G. Siegl, P. Bettini, J.-M. Noterdaeme, and K. Crombé

Review of Scientific Instruments ARTICLE scitation.org/journal/rsi

Development of an experimental facility for the study of microparticle initiated radio frequency vacuum breakdown

Cite as: Rev. Sci. Instrum. 92, 013508 (2021); doi: 10.1063/5.0034559
Submitted: 21 October 2020 • Accepted: 23 December 2020 •
Published Online: 21 January 2021

R. Casagrande,[1,2,3,a] H. Faugel,[2] F. Fischer,[2] H. Fünfgelder,[2] F. Riedl,[2] G. Siegl,[2] P. Bettini,[3] J.-M. Noterdaeme,[1,2] and K. Crombé[1,4]

AFFILIATIONS

[1] Department of Applied Physics, Ghent University, 9000 Gent, Belgium
[2] Max-Planck-Institut für Plasmaphysik, 85748 Garching, Germany
[3] Università degli Studi di Padova, 35122 Padova, Italy
[4] Laboratory for Plasma Physics, ERM/KMS, 1000 Brussels, Belgium

[a] **Author to whom correspondence should be addressed:** riccardo.casagrande@ipp.mpg.de

ABSTRACT

An ongoing objective in the ion cyclotron range of frequencies (ICRF) systems is the improvement of power coupling to the plasma. During the last decade, this goal has been mainly pursued through the study of the coupling resistance, either by optimizing the antenna layout or by tailoring the scrape-off layer profile with gas puffing. Another approach is to increase the voltage handling capability of the ICRF system, limited by breakdown in the launchers or in the transmission lines. This paper describes the design of the ICRF Breakdown EXperiment (IBEX), a device to investigate fundamental aspects of radio frequency arcs under ICRF-relevant conditions. IBEX can achieve a peak voltage of 48 kV at 54 MHz with a 5 kW input power.

I. INTRODUCTION

In next generation fusion devices, in order to meet the tritium breeding ratio requirements, heating systems with reduced impact on the breeder volume will be required.[1] If the port-plug antenna design adopted for ITER is maintained for future reactors, the requirement of a small footprint will inevitably lead to high power density launchers and, in turn, to high voltages on the ion cyclotron range of frequency (ICRF) system. The ITER antenna, coupling 20 MW to the plasma in the 40 MHz–55 MHz frequency range, will have a maximum voltage on the straps[2] in excess of 40 kV. In the case of an in-port solution for DEMO, electric field limits will also be major design issues. It is then desirable to extend the range of operational voltage and electric field in ICRF systems not only to reduce the design complexity but also to improve the reliability of antennas.

A device dedicated to the study of fundamental mechanisms of radio frequency arcs has been developed at the Max-Planck-Institut für Plasmaphysik in Garching, Germany, with the aim of gaining improved information on voltage limits of ICRF launchers. In this paper, we describe the design of ICRF Breakdown Experiment (IBEX) particularly focusing on the development of an RF system able to meet the voltage and frequency requirements.

II. ICRF ENVIRONMENT

A. Operational limits

The voltage limit imposed by the ITER Organization (IO) on the ICRF system is 45 kV with a maximum electric field of 2 kV/mm along the magnetic field lines and 3 kV/mm on all the other locations.[2] These boundaries are extrapolated from the operational conditions of existing antennas, and hence, the strategy to ensure reliability and availability is to provide a reasonably large margin on the main macroscopic parameters affecting the breakdown in known systems. However, arcs in ICRF antennas are still poorly understood due to the complexity and the range of spurious interactions the tokamak environment can give rise to and the difficulty of direct observation and diagnosis of breakdown inside the antenna box.

Significantly higher electric fields, with respect to the ones established by IO, are routinely achieved in closed vacuum environments, e.g., RF cavities for particle accelerators, where extremely good control over the surface conditions can be obtained. Conversely, ICRF launchers can be subjected to dust contamination due to the erosion of plasma-facing components, as well as plasma interaction during intense transient events such as Edge Localized Modes (ELMs).[3] Studies on the effect of plasma interaction on the voltage stand-off have been carried out in ASDEX Upgrade with an RF probe,[4] providing some insight into the observed correlation between ELMs and antenna breakdown. On the other hand, the effect of microparticles on the voltage holding of ICRF launchers has not been explored in detail yet, concerning both particulate contamination and dust impact on the antenna.

B. Dust deleterious effects

Microparticles are well known to affect the voltage holding of vacuum insulated gaps, either by producing enhanced field emission sites if deposited on the electrodes surface or by being accelerated by the background electric field, which, in turn, can lead to the evaporation of the particle or the formation of craters upon impact with the electrodes.[5] The latter is usually not a relevant phenomenon in RF structures, since the charge to mass ratio of typically encountered particles does not allow for enough acceleration during the half RF period. Nonetheless, large amounts of particulate are generated in nuclear fusion reactors,[6–8] which can reach the ICRF launchers. Microparticles can be remobilized and deposited on the antenna surface or subjected to acceleration in the edge plasma, reaching velocities up to several hundreds of m/s prior to the vaporization or impact with the plasma-facing components.[9] IBEX aims at providing a test platform to investigate the parameters that can influence voltage holding, specifically under ICRF relevant conditions, focusing on microparticle contamination during the initial experimental phase.

III. EXPERIMENT SPECIFICATIONS

A. Main requirements

The main requirement of IBEX is to provide voltage and electric field conditions at the test electrodes at and above the typical limits of ICRF systems. Since these values can greatly vary between different machines, the limitations on ITER ICRF were considered as design basis. Other requirements include the background pressure well below the typical observed limits for the modified multipactor discharge, i.e., less than 10^{-4} mbar.[10] IBEX should also guarantee a quick replacement of the test electrodes and have the possibility to interface with a microparticle injection system.

B. Experiment outline

High voltages in the frequency range of interest can be obtained by generating a standing wave pattern in a coaxial transmission line. The maximum voltage standing wave ratio (VSWR) is achieved under resonant conditions: in IBEX, a $\lambda/4$ coaxial resonator is used to obtain a high RF voltage on the test electrodes, positioned at the open end. The terminal part of the resonator is composed of a vacuum piping section and connected to a pumping system to achieve experimental pressures below 10^{-4} mbar. Vacuum tightness and electrical continuity are ensured by a coaxial ceramic feedthrough in the initial segment of the transmission line. A linear manipulator allows the precise adjustment of the electrodes gap. Several access ports are available in the test chamber to provide a direct view on the electrodes and an interface with the microparticle accelerator. The experiment is powered through a 5 kW solid-state amplifier (SSA) connected to the feeding point via the following:

- RF switch, which allows the connection of a network analyzer to the resonator to perform the tuning procedure.
- Directional coupler, which monitors forward and reflected power.
- Bias tee, which guarantees electrical separation between the DC and RF circuit. This allows the DC biasing of the transmission line (e.g., for glow discharge conditioning) and measurement of the rectified field emission current, other than providing protection to the SSA.

The RF voltage and current in the resonator are monitored through capacitive and inductive probes. For impedance matching, a variable vacuum capacitor is used. Figure 1 shows the basic outline of IBEX.

IV. GENERATION OF HIGH RF VOLTAGE

A. Quality factor and standing wave maximum

A key aspect in the design of IBEX was the maximization of the voltage on the test electrodes, given the limited 5 kW input power (P_i). In a quarter wavelength coaxial resonator (Fig. 2) with constant characteristic impedance (Z_0), assuming a perfect matching with the source output impedance and a total reflection of the wave at the extremes, the peak voltage at the open end can be estimated as

$$V_{open} = \sqrt{\frac{8P_iQZ_0}{\pi}}. \quad (1)$$

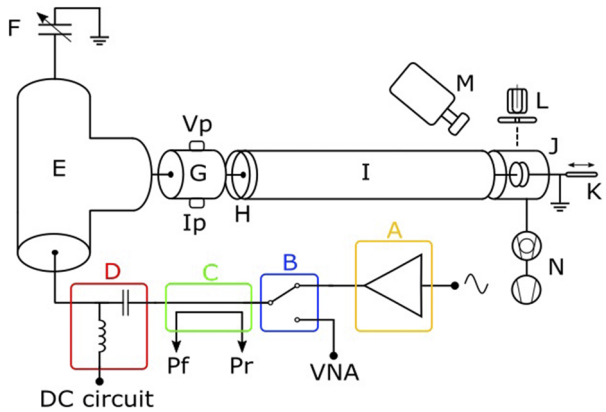

FIG. 1. IBEX schematic representation. A—solid-state amplifier, B—RF switch, C—directional coupler, D—bias tee E—9″ transmission line T section, F—tuning vacuum capacitor, G—voltage and current probes, H—vacuum feedthrough, I—high impedance transmission line section, J—test electrodes, K—linear manipulator, L—microparticle source, M—high speed camera, and N—pumping system.

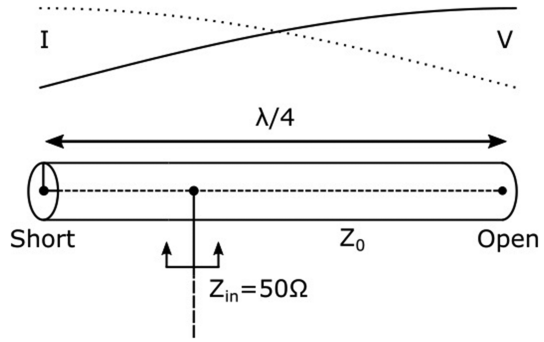

FIG. 2. Voltage and current distribution in a quarter-wavelength coaxial resonator.

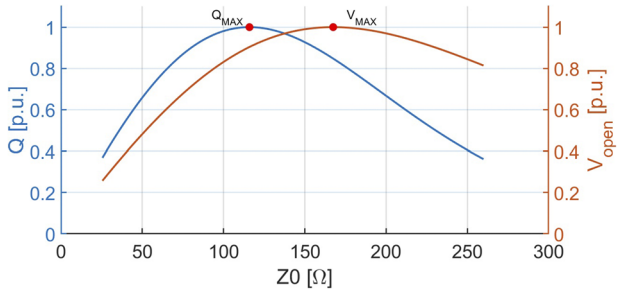

FIG. 3. Z_0 dependence of the Q factor and open-end voltage in a $\lambda/4$ coaxial resonator.

The maximization variables for V_{open} are then the characteristic impedance and the quality factor (Q). Q represents the ratio between the stored and dissipated energy in a RF cycle. For a coaxial transmission line with phase constant β and attenuation constant α, the value of Q arising from resistive losses in the conductors is

$$Q_{TL} = \frac{\beta}{2\alpha} = \frac{2\pi}{\lambda R_{TL}}, \tag{2}$$

with R_{TL} being the resistance per unit length of the transmission line. In IBEX, the main contribution in terms of power losses per RF cycle comes from the vacuum section of the resonator, since it is composed of stainless steel piping segments with an inner diameter of 153 mm acting as the outer conductor. To minimize losses and to achieve good vacuum compatibility, the inner conductor material was chosen to be oxygen-free copper. The resistance per meter of the mixed-material coaxial line can be expressed as

$$R_{TL} = \sqrt{\frac{f\mu_0}{\pi}}\left(\frac{\sqrt{\mu_{in}\rho_{in}}}{d_{in}} + \frac{\sqrt{\mu_{out}\rho_{out}}}{d_{out}}\right), \tag{3}$$

with d, μ, and ρ being the diameter, permeability, and resistivity, respectively, and subscripts identifying the inner or outer conductor. The lower conductivity of the coaxial line outer conductor is not extremely penalizing in terms of power losses due to the larger penetration depth and cross sectional area. Z_0 = 116 Ω yields the optimal unloaded Q, although the maximum voltage at the resonator open end, given by Eq. (1), is achieved with a lower quality factor for a characteristic impedance of 167 Ω (Fig. 3). Therefore, the vacuum section of the transmission line [Fig. 1(I)] must have a high characteristic impedance, hereinafter referred to as $Z_{0,vs}$.

B. Matching network

For maximum power transfer, the input impedance of the resonator needs to be matched to the 50 Ω output of the amplifier (Z_{amp}). In IBEX, this is performed with a variable vacuum capacitor connected in parallel to the open-ended coaxial line. The reactance seen from the feeding point can be increased by adding a section of the transmission line (shorter than $\lambda/4$) in series with the vacuum capacitor, thus reducing its contribution to the matching capacitance and therefore increasing Q.

Referring to the scheme in Fig. 4, resonance and matching are achieved for the following condition:

$$\begin{aligned} Y_{in} &= \frac{1}{Z_{amp}} = Y_{vs} + Y_{mn} \\ &= Y_{vs}\tanh(\gamma_{vs}L_{vs}) + \frac{j\omega C_{tun} + Y_{mn}\tanh(\gamma_{mn}L_{mn})}{Y_{mn} + j\omega C_{tun}\tanh(\gamma_{mn}L_{mn})}. \end{aligned} \tag{4}$$

L, γ, Z_0, and Y are the length of the transmission line, its propagation constant, its characteristic impedance, and the admittance, respectively, seen from the reference points in Fig. 4. Subscripts denote the matching network, vacuum section, and input.

For a fixed length of the transmission lines, Eq. (4) has two solutions. The maximum Q in this configuration is always achieved for the higher of the two resonant frequencies. Figure 5 represents how the matching condition is reached.

C. Circuit analysis

The actual IBEX setup is more complex than the simplified schemes used for preliminary design considerations in Secs. IV A and IV B. The presence of a lumped tuning capacitor, changes in characteristic impedance, and ceramic supports do not allow for a direct evaluation of the maximum voltage with Eq. (1). To study the resonator behavior and predict the maximum achievable voltage in the realistic setup, a circuit model was developed in QucsStudio.[11]

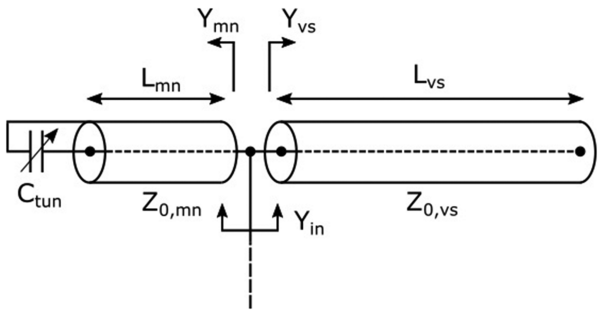

FIG. 4. Schematic representation of the resonator and matching network.

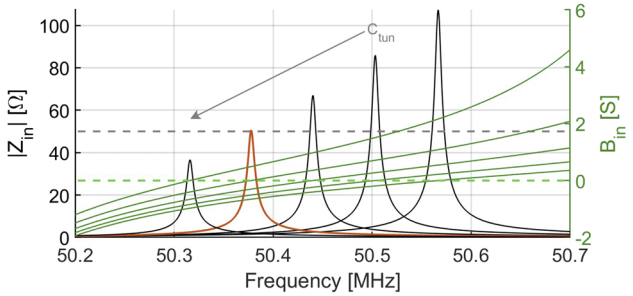

FIG. 5. Approaching the resonant and maximum power transfer conditions through variation of the tuning capacitance. C_{tun} is varied stepwise until the input susceptance (B_{in}) is zero. Maximum power transfer is achieved when the input impedance at resonance equals Z_{amp}.

Given a fixed physical length of the transmission lines, the resonant frequency and the open-end voltage were investigated depending on the characteristic impedance of the vacuum section and the capacitance introduced by the test electrodes. Matching was achieved through the minimization of S11 using the tuning capacitance as the optimization variable. With respect to the optimal characteristic impedance estimated in Sec. IV A, the maximum voltage in the realistic configuration is achieved at higher $Z_{0,vs}$ (Fig. 6). Due to mechanical constraints, a compromise had to be made between maximization of the open-end voltage and sufficient support of the inner conductor, which is cantilevered from the ceramic feedthrough. The inner conductor diameter in the vacuum section of the resonator was thus chosen to be 12 mm, leading to a characteristic impedance of 153 Ω.

The electrode capacitance (C_{el}) can also significantly influence the Q factor, and thus, the peak voltage is achievable. In particular, the resistance to ground (R_{gnd}) plays a major role in the system performance when considering the capacitance introduced by the test electrodes. For higher C_{el}, the leakage current to ground is increased, reducing the Q factor with a magnitude that depends on R_{gnd}. When the capacitance of electrodes becomes sufficiently small, Q stabilizes to a value depending on the quality factor of the tuning capacitor and transmission line; this threshold is also conditioned by the resistance to ground (Fig. 7).

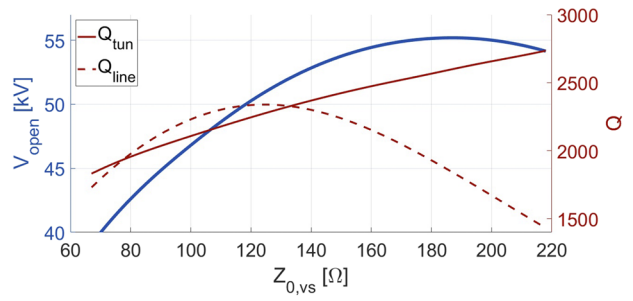

FIG. 6. Simulated voltage at the open-end of the resonator and Q factor of the transmission line and tuning capacitor as a function of $Z_{0,vs}$ for 5 kW input power.

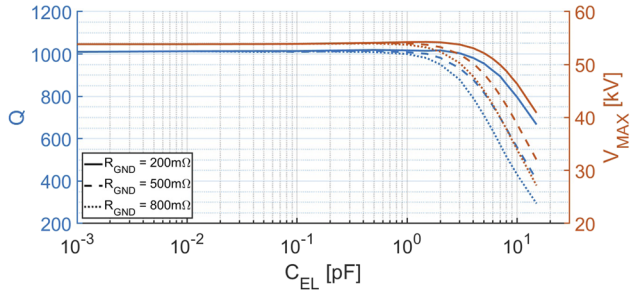

FIG. 7. Dependence of the quality factor and open-end voltage on C_{EL} and R_{GND} for $Z_{0,vs}$ = 153 Ω.

V. MICROPARTICLE SOURCE

A. Requirements

Microscopic dust particles are produced in all magnetic confinement fusion devices due to plasma/surface interactions. Dust dynamics can be significantly affected by the edge plasma, accelerating the particles to mean velocities exceeding 100 m/s.[12] Hypervelocity dust impact events have been recorded in tokamaks, even though at a lower rate, indicating that microparticles can reach velocities >1 km/s.[13,14] Dust analysis in several machines indicate that a dominant fraction of the particles consists of plasma-facing materials, with the morphology varying from spheroids to irregular shapes.[7] Theoretical modeling and experimental evidence indicate that microparticles accelerated in a high voltage vacuum gap can trigger the breakdown through a variety of processes. Microparticle injection experiments, at both hypervelocity[15] and low velocity,[16] defined a range of microparticles parameters for which the trigger discharge is most likely to occur. Considering the typical dust size and velocity observed in tokamaks, experimental findings regarding microparticle triggered discharges, and ICRF antennas materials, the set of parameters in Table I have been defined for particle injection studies in IBEX.

B. Design of the dust source

For particle acceleration up to the velocity range defined in Table I, an electrostatic source[17] was developed. A reservoir containing the microparticles and a microtip is kept at a high potential. A beam triode allows us to switch the reservoir potential to ground. During this phase, the dust is lifted inside the chamber, with a fraction depositing on the charging tip. Here, the microparticles acquire a high charge and upon detachment from the tip are accelerated through a pinhole aperture in the reservoir. A grounded extraction plate completes the acceleration, leading to an einzel lens for beam focusing. For a charging tip of radius r_T and a particle of radius

TABLE I. Parameters for microparticle injection studies.

Electrode material	Stainless steel
Microparticles' composition	Tungsten
Microparticles' velocity	<1000 m/s
Microparticles' size	0.5 μm–30 μm

$r_P < r_T$, the velocity acquired by the microparticle can be estimated[18] as in the following equation:

$$v_P = \frac{\pi V}{r_P + r_T}\sqrt{\frac{\varepsilon_0}{\rho}\frac{r_T}{r_P}}. \quad (5)$$

This assumes, as in the setup above, that the accelerating and charging voltages (V) are equal. Figure 8 shows the maximum velocities achievable by tungsten microparticles, accelerated by a 25 kV potential. The experimentally observed velocities are, in general, lower than the estimate given by Eq. (5) due to the incomplete charging of particles.

The charging voltage is limited by field emission and field evaporation, respectively, for negative and positive charging.[19] Field evaporation of tungsten at room temperature occurs in the 5 MV/Å range, whereas discharge of the microparticle due to field emission happens at one order of magnitude lower electric fields. To achieve higher charging (and accelerating) potential and to reduce the breakdown probability, microparticles are charged positively. The maximum charging voltage achievable, given the field evaporation limit of 5 MV/Å (E_{ev}), is

$$V_{max} = \frac{E_{ev} r_T}{k} \quad (6)$$

in which k is an amplification factor depending on rT/rP. For the smallest microtip radius considered (5 μm) and the highest rT/rP, the absolute voltage limit is 100 kV. The actual constraint in terms of potential is instead defined by the pulse modulating triode capable of handling a maximum voltage of 30 kV.

VI. TEST ELECTRODES

A. Electrodes for microparticle deposition experiments

Plane-parallel electrode configuration was chosen to investigate the effect of microparticle contamination on the breakdown rate. This geometry allows for simple surface preparation with standard grinding and polishing metallographic techniques. Given the performances foreseen for IBEX in terms of maximum voltage and experimentally observed RF breakdown fields in vacuum,[20] the gap considered is below 2.5 mm. For an electrode diameter of 40 mm and the aforementioned spacing, the field enhancement at the edges is not extremely pronounced. Therefore, a Borda profile was chosen to minimize the edge effect (Fig. 9) and to maintain a more compact footprint with respect to Rogowski and Bruce profiles. A smaller size was desirable to lower the stress on the cantilevered inner conductor of the resonator and due to limitations on the sample dimensions allowed in the Scanning Electron Microscope (SEM).

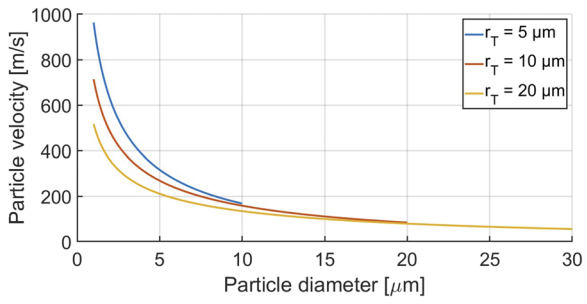

FIG. 8. Maximum velocity of microparticles for V = 25 kV.

B. Electrodes for microparticle injection experiments

To provide an impact surface for the microparticles injected from the dust accelerator, which is installed orthogonally with respect to the axis of the resonator, a point–plane electrode configuration is used. The pointed electrode is a truncated cone terminating in a 2 mm diameter hemisphere. Figure 10 represents the two geometries chosen for experiments.

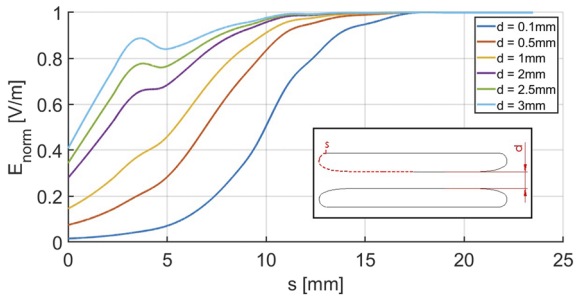

FIG. 9. Normalized surface electric field distribution for different electrode spacings.

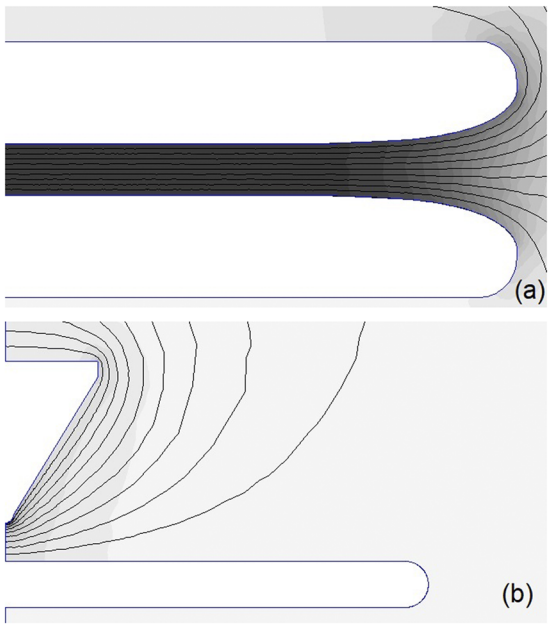

FIG. 10. Test electrodes.

C. Capacitance of the test electrodes

Following the considerations of Sec. IV C, the capacitance of the two electrode configurations has been computed with the finite element method (Fig. 11).

Due to the small surface area, Q factor degradation can be neglected for the point–plane configuration. On the other hand, the plane-parallel electrodes introduce a large capacitance for the whole range of spacings considered. To avoid a significant decrease in performance, particular care will need to be taken for the minimization of the RF resistance to ground in the case of microparticle deposition experiments.

VII. DIAGNOSTIC FOR FIELD EMISSION CURRENT

A. Field emission current in RF regime

For a sufficiently high surface electric field, electrons can tunnel through the potential barrier and give rise to a field emitted current. In high voltage vacuum systems, this current controls fundamental parameters of arc formation such as field emitter evaporation and Coulomb explosion, thus playing a major role as a precursor to the breakdown.[21] The Fowler–Nordheim expression provides the field emission current density for a given work function (ϕ), macroscopic electric field (E), and enhancement factor (β). The simplified expression given by Wang and Loew[22] reads

$$j_{FE} = \frac{1.54 \cdot 10^{-6} \cdot 10^{4.52\phi^{-0.5}} (\beta E)^2}{\phi} \exp\left(\frac{-6.53 \cdot 10^{9} \phi^{1.5}}{\beta E}\right). \quad (7)$$

Since the tunneling time is extremely short with respect to the RF period, it can be assumed that the field emission process is the same as in the DC regime. Thus, if a time-varying electric field is applied to a plane-parallel electrode configuration, the current will be field emitted alternately from the two electrodes for the negative half period, responding to the instantaneous electric field. If contaminants are introduced, there is a probability that they will turn into field emitters, thus increasing β—and emitting area—for a specific electrode.

B. Current-measurement circuit

To measure the field emission current in the nA range, a device consisting of a low-pass filter followed by a high gain transimpedance amplifier was developed. The voltage output—proportional to the average field emission current over one RF period—is then monitored through a low noise multimeter with a large dynamic range. The current-measurement circuit is connected to the resonator through the bias tee [Fig. 1(D)], which provides RF insulation. The additional low-pass filter is used prior to the transimpedance amplifier to reduce the RF input signal below the noise floor level. Given the extreme sensitivity of field emission on the local electric field, a variation of 1% between the two β already leads to a negligible current emitted from the electrode with the lower value (Fig. 12). In principle, it will thus be possible to discriminate the field emitting electrode with this setup.

VIII. PRELIMINARY TESTS ON IBEX

A. Measurement of Q factor

Quality factor measurements were carried out on IBEX to compare the simulated results with the actual setup performances. The loaded Q was computed from the S_{11} parameter measured with a network analyzer. The central frequency is determined from the minimum of S_{11} amplitude, whereas the −3dB points are found as the maximum and minimum of the S_{11} imaginary part after the correction of the phase offset in the Smith chart. The maximum Q factor, i.e., measured without the loading effect introduced by the electrodes capacitance, is 830. This value is 83% of the simulated Q, leading to a reduction of 10% on the maximum achievable voltage at the open end with respect to the value obtained from circuit analysis.

B. RF resistance to ground

The Q factor of the resonator was measured for varying C_{EL} to investigate the effect of its degradation in relation to the magnitude of the RF resistance to ground. To observe the effect over a large range of capacitances, two electrodes sets have been used:

- Plane-parallel electrodes: $C_{EL} \gtrsim 1$ pF.
- Plane-sphere electrodes: $C_{EL} \lesssim 1$ pF.

Figure 13 shows the measured Q factor in comparison with the results obtained from simulations. Referring to the capacitance of

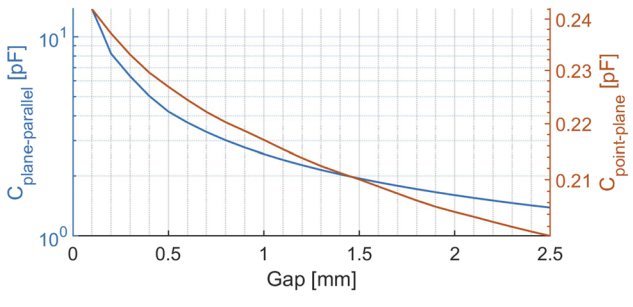

FIG. 11. Electrode capacitance for the two configurations considered.

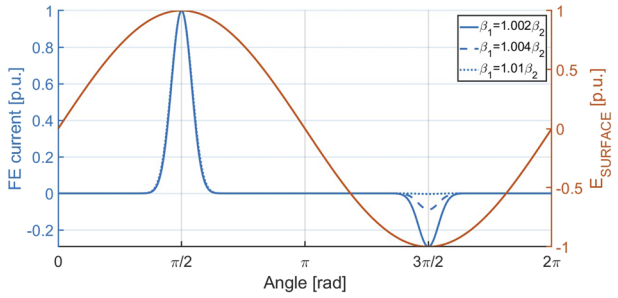

FIG. 12. Field emission current during one RF period on a plane-parallel configuration with different β on the two electrodes.

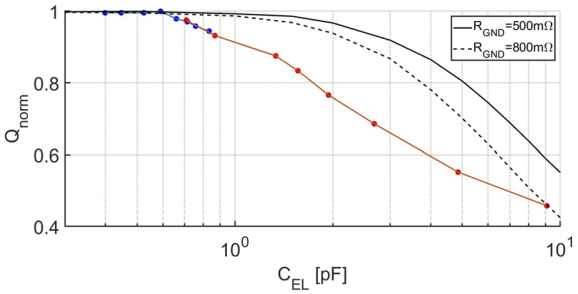

FIG. 13. Measured Q factor with varying electrodes capacitance and comparison with the simulated values.

the test electrodes considered (Fig. 11), it is clear that for the plane-parallel configuration, the RF resistance to ground will need to be reduced to avoid excessive degradation of Q.

C. Multipactor

The multipactor can be used as a conditioning tool to remove adsorbed contaminants from the electrodes. The currents generated from the ionization of the desorbed gases, which affect the field emission measurements, can then be suppressed.

The multipactor has been characterized for IBEX under resonant conditions and 50 Ω matching at a low input power by monitoring the forward and reflected power, pressure, electron current collected from a positively biased probe, and total current flowing through the bias-tee DC circuit. Electron resonance is observed for an input range of 2.5 W–17 W. After the onset of the multipactor, the input power is almost entirely reflected, accompanied by an increase in pressure. A current increasing with the power applied is observed both at the electron probe (Fig. 14) and through the DC circuit of the bias tee. At higher power levels, in the 300 W–500 W range, a small current flowing in the opposite direction with respect to the multipactor case is measured at the bias tee without the increase in reflected power; a pressure surge is observed, but of smaller magnitude compared to the multipactor conditions. This phenomenon is probably correlated with desorption and subsequent ionization of the gases.[23]

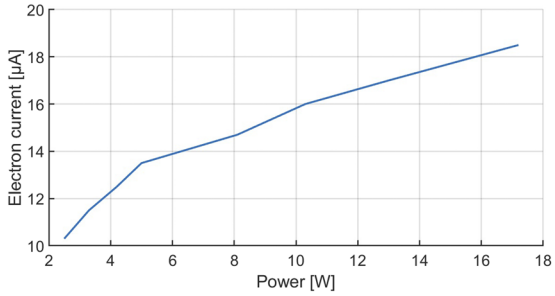

FIG. 14. Multipactor current measured with an electron probe biased at 100 V and positioned at the open-end of the resonator.

IX. CONCLUSION

We have designed and built a device for the fundamental study of RF vacuum breakdown in the application to ICRF antennas. The facility is able to produce a peak voltage of 48 kV with variable electrode gap spacing at a frequency of 54 MHz. Experimental work will be focused on the effect of particulates commonly observed in magnetic confinement fusion devices on voltage holding and the associated field emission current.

ACKNOWLEDGMENTS

This work was carried out with the support of Ghent University—Department of Applied Physics, and the Max Planck Institute for Plasma Physics.

DATA AVAILABILITY

The data that support the findings of this study are available from the corresponding author upon reasonable request.

REFERENCES

[1]J.-M. Noterdaeme, A. Messiaen, R. Ragona, W. Zhang, A. Bader, F. Durodié, U. Fischer, T. Franke, E. Smigelskis, J. Ongena, M. Q. Tran, D. Van Eester, and M. Van Schoor, "Progress on an ion cyclotron range of frequency system for DEMO," Fusion Eng. Des. **146**, 1321–1324 (2019), part of the Special Issue: SI:SOFT-30.

[2]F. Durodié, M. Vrancken, R. Bamber, L. Colas, P. Dumortier, D. Hancock, S. Huygen, D. Lockley, F. Louche, R. Maggiora, D. Milanesio, A. Messiaen, M. P. S. Nightingale, M. Shannon, P. Tigwell, M. Van Schoor, D. Wilson, K. Winkler, and C. Team, "Performance assessment of the ITER ICRF antenna," AIP Conf. Proc. **1580**, 362–365 (2014).

[3]G. Federici, "Plasma wall interactions in ITER," Phys. Scr. **2006**(T124), 1–8.

[4]V. Bobkov, J.-M. Noterdaeme, F. Wesner, R. Wilhelm, and ASDEX Upgrade Team, "Influence of the plasma on ICRF antenna voltage limits," J. Nucl. Mater. **313-316**, 956–961 (2003), part of the Special Issue: Plasma-Surface Interactions in Controlled Fusion Devices 15.

[5]R. Latham, *High Voltage Vacuum Insulation: Basic Concepts and Technological Practice* (Elsevier Science, 1995).

[6]V. Rohde, M. Balden, T. Lunt, and ASDEX Upgrade Team, "Dust investigations at ASDEX upgrade," Phys. Scr. **2009**(T138), 014024.

[7]M. Balden, N. Endstrasser, P. W. Humrickhouse, V. Rohde, M. Rasinski, U. von Toussaint, S. Elgeti, and R. Neu, "Collection strategy, inner morphology, and size distribution of dust particles in ASDEX upgrade," Nucl. Fusion **54**, 073010 (2014).

[8]A. Autricque, "Dust transport in tokamaks," Ph.D. thesis, Aix-Marseille, 2018.

[9]R. Smirnov, S. Krasheninnikov, A. Pigarov, D. Benson, M. Rosenberg, and D. Mendis, "Modeling of velocity distributions of dust in tokamak edge plasmas and dust–wall collisions," J. Nucl. Mater. **390-391**, 84–87 (2009), part of the Special Issue: Proceedings of the 18th International Conference on Plasma-Surface Interactions in Controlled Fusion Device.

[10]F. Höhn, W. Jacob, R. Beckmann, and R. Wilhelm, "The transition of a multipactor to a low-pressure gas discharge," Phys. Plasmas **4**, 940–944 (1997).

[11]M. Margraf, Qucsstudio—A free and powerful circuit simulator.

[12]F. Brochard, V. Rohde, T. Lunt, G. Suárez López, A. Shalpegin, and R. Neu, "Intrinsic dust transport in ASDEX upgrade studied by fast imaging," Nucl. Mater. Energy **18**, 268–274 (2019).

[13]S. Ratynskaia, C. Castaldo, K. Rypdal, G. Morfill, U. de Angelis, V. Pericoli-Ridolfini, A. Rufoloni, and E. Giovannozzi, "Hypervelocity dust impacts in FTU scrape-off layer," Nucl. Fusion **48**, 015006 (2008).

[14]M. Tang, J. S. Hu, J. G. Li, Y.-F. Li, G. Morfill, and N. Ashikawa, "Recent researches on dust in EAST and HT-7 tokamaks," J. Nucl. Mater. **415**, S1094–S1097 (2011).

[15]J. C. Slattery, J. F. Friichtenicht, and D. O. Hansen, "High-voltage breakdown initiated by particle impact," Appl. Phys. Lett. **7**, 23–25 (1965).

[16]A. K. Chakrabarti and P. A. Chatterton, "Microparticle trigger discharges and impact damage in a high-voltage vacuum insulated gap," J. Appl. Phys. **47**, 5320–5328 (1976).
[17]M. Stübig, G. Schäfer, T.-M. Ho, R. Srama, and E. Grün, "Laboratory simulation improvements for hypervelocity micrometeorite impacts with a new dust particle source," Planet. Space Sci. **49**, 853–858 (2001), part of the Special Issue: Asteroids, Meteorites, Impacts and their Consequences (AMICO 2000).
[18]H. Shelton, C. D. Hendricks, Jr., and R. F. Wuerker, "Electrostatic acceleration of microparticles to hypervelocities," J. Appl. Phys. **31**, 1243–1246 (1960).
[19]T. Trottenberg, H. Kersten, and H. Neumann, "Feasibility of electrostatic microparticle propulsion," New J. Phys. **10**, 063012 (2008).
[20]R. L. Kustom, "Effect of radio-frequency fields on the electrical breakdown of vacuum-insulated electrodes," J. Appl. Phys. **41**, 3256–3268 (1970).
[21]H. Timko, K. Ness Sjobak, L. Mether, S. Calatroni, F. Djurabekova, K. Matyash, K. Nordlund, R. Schneider, and W. Wuensch, "From field emission to vacuum arc ignition: A new tool for simulating copper vacuum arcs," Contrib. Plasma Phys. **55**, 299–314 (2015).
[22]J. Wang and G. Loew, "Field emission and RF breakdown in high-gradient room temperature linac structures," Technical Report No. SLAC-PUB-7684, Stanford University, Stanford Linear Accelerator Center, CA, USA, 1997.
[23]J. Tan, H. Safa, B. Bonin, and J.-M. Tessier, "Radiofrequency field-emission studies. I: Design of a microwave cavity," J. Phys. D: Appl. Phys. **27**, 2644 (1994).